BULLETIN OF THE POLISH ACADEMY OF SCIENCES
TECHNICAL SCIENCES, Vol. 72(2), 2024, Article number: e148874
DOI: 10.24425/bpasts.2024.148874

Non-bifurcation behavior of laminated composite plates under in-plane compression

Mehdi BOHLOOLY FOTOVAT* **and Tomasz KUBIAK**

Department of Strength of Materials, Lodz University of Technology, Stefanowskiego 1/15, 90-537 Lodz, Poland

Abstract. The paper deals with bifurcation and/or non-bifurcation post-buckling curves of composite plates under biaxial compression. For different lay-up sequences, a coupling, i.e. extension-bending (EB) is considered. The current investigations present distinct equilibrium paths describing when they have bifurcation-type and/or non-bifurcation-type responses. The novel parameter (i.e. EB coupling imperfection) is calculated to show the amount of non-bifurcation in the equilibrium path as a quantitative parameter. For the case of non-square plates, a novel mixed-mode analysis is conducted. The effects of different characters in laminated composites such as layer arrangement, loading ratio, aspect ratio, and boundary conditions are investigated. A novel result concluded in the numerical examples where there are some possibilities to have different mode shapes in linear and non-linear buckling analysis. FEM results of ANSYS software verify the results of analytical equations.

Keywords: non-bifurcation equilibrium path; laminates; antisymmetric; extension-bending.

1. INTRODUCTION

Unlike traditional isotropic materials, the next generations may have some complexities in their modelling and analysis. As it is well known, according to classical lamination theory, the couplings between different pairs of behaviors, e.g. “extension”, “shearing”, “bending” and “twisting" can exist. Herein, the couplings between extension and bending were the scope of the current study. Such coupling comes when the material distribution has no symmetry to the middle plane of the structure. According to the classical lamination theory for thin-walled structures, this non-symmetry causes a coupling behavior in which exposing in-plane loads leads a structure to undergo deflection and vice versa. This is the main reason for observing the non-bifurcation equilibrium path in the initial post-buckling for plates under in-plane compressions.

There are a large number of materials that violate the symmetry across the thickness. One of the familiar cases is functionally graded materials (FGMs), in which ceramic and/or steel volume fractions may vary through thickness [1]. Reinforcing structure by adding a stiffener on one side of the structure (eccentrically stiffened) may cause a coupling between extension and bending [2]. A ubiquitous lightweight material with the ability to have such a coupling is laminated composites where lay-up sequence is vital in this field [3]. An analogous situation is observed for materials that are much newer, such as nanotube-reinforced composites [4], shape memory alloys [5], heterogeneous auxetic [6], and so on. To tackle this problem, such materials can be considered as a symmetric structure (e.g. for FGM [7, 8] and graphene platelet [9–11]). However, the problem persists in the case of unsymmetric cases and there is a need to define a quantitative parameter to describe coupling effects on the non-bifurcation equilibrium path. This paper tries to define a parameter for laminated composite plates for the first time in literature. Also, it can be useful for other types of unsymmetric materials.

According to the literature review, some investigators stated that there is no bifurcation point for unsymmetric structures under compression. Due to the presence of coupling (i.e. “extension-bending” or “stretching-bending”), by applying a low value of in-plane load, the deflection starts to grow. Such studies were based on numerical methods like the finite element method [12] or finite strip method [13]. Also, this condition can be seen in time-dependent loads, where deflection is non-zero before dynamic buckling [14]. Lal *et al.* [15] added the possibility of eigenvalue/bifurcation in the case of unsymmetric laminates, in which the bending-extension coupling coefficients become zero when in-plane loads coincide with the neutral plane. Zhang [16] presented the thermal post-buckling of FGM beams based on a physically neutral surface. In contrast to these reports [12–14], some other investigators show that there is a bifurcation-type equilibrium path in the presence of extension-bending coupling. Huang and Han [17, 18] investigated the static and dynamic response of the FGM cylindrical shell. Duc *et al.* presented the post-buckling behavior of stiffened FGM for plates [19], shells [20], and panels [21]. Bich *et al.* [22] worked on the non-linear response of FGM shallow spherical shells under combined thermal and mechanical loads. Sofiyev *et al.* [23] studied the non-linear buckling of laminated conical shells by non-symmetric layer arrangement. Bohlooly and Malekzadeh Fard [24] presented the post-buckling of rectangular plates with general laminates and considered a concentric stiffener. Foroutan and Dai [25] examined the static and dynamic analysis of sigmoid FGM cylindrical shells. Zhu *et al.* [26] per-

*e-mail: mehdi.bohlooly-fotovat@p.lodz.pl

Manuscript submitted 2023-07-27, revised 2023-11-28, initially accepted for publication 2023-12-18, published in March 2024.

formed electro-thermo-mechanical post-buckling of the FGM cylindrical shell while considering piezoelectric layers. In references [17–26], the equilibrium and compatibility equations are derived based on deflection and a stress function. The solution is based on the Galerkin method, which gives a closed-form solution in static loads, and it is expeditious in dynamic analysis compared to numerical ways. Such benefits led investigators to present work (much of which is not cited here) on different types of materials, geometries, static/dynamic loads, etc. This method gives reliable results for symmetric structures. However, the contradictory result between numerical [12,13] and the Galerkin methods [17–26] is a serious mystery. Therefore, an attempt is made to find out the main reason for non-bifurcation post-buckling curves in the presence of the EB coupling matrix in the current investigation.

The novelty of this paper is defining an analytical parameter that shows the amount of non-bifurcation of initial post-buckling curves in the presence of EB coupling. In this regard, three closed-form equilibrium equations are derived for a simply supported rectangular plate under biaxial compression. First, the analytical formulation of laminated composites based on the Galerkin method is repeated from the available literature. It gives a bifurcation-type equilibrium path. Second, it is improved by the virtual displacement principle by using novel terms in the equilibrium equation and the same deflection function in the first step. It provides a non-bifurcation-type equilibrium path. However, it is accurate for only square plates. Third, a novel mixed mode of deflection function is considered suitable for non-square plates. It is found that the boundary condition has a vital role in the bifurcation-type or non-bifurcation-type equilibrium path. The solutions without satisfying such boundary conditions yield inaccurate computations for non-symmetric lay-up sequences. It is decided to fulfill these conditions by assuming an artificial rotational spring. This assumption causes additional terms in the equilibrium equations. The amount of non-bifurcation is demonstrated by a novel quantitative EB coupling imperfection. The effects of different characters like lay-up sequence, loading ratio, aspect ratio, and boundary conditions are investigated. In all numerical results, the results of the present study are verified by FEM in ANSYS.

2. ANALYTICAL SOLUTION

A plate is composed of laminated composite in this study. The plate of length a, width b, and thickness h and the Cartesian coordinate system (x, y, z) are shown in Fig. 1. The four edges of the plate are considered movable and simply supported and they are subjected to biaxial compression with a loading ratio R which equals P_y/P_x. Both boundary conditions and in-plane loads coincide in the middle plane $(z = 0)$.

Based on classical lamination theory, the resultants of force N and moment M can be written in a relationship between mid-plane strains ε^0 and curvatures κ by

$$\begin{bmatrix} \mathrm{N} \\ \mathrm{M} \end{bmatrix} = \begin{bmatrix} \mathrm{A} & \mathrm{B} \\ \mathrm{B} & \mathrm{D} \end{bmatrix} \begin{bmatrix} \varepsilon^0 \\ \kappa \end{bmatrix}, \tag{1}$$

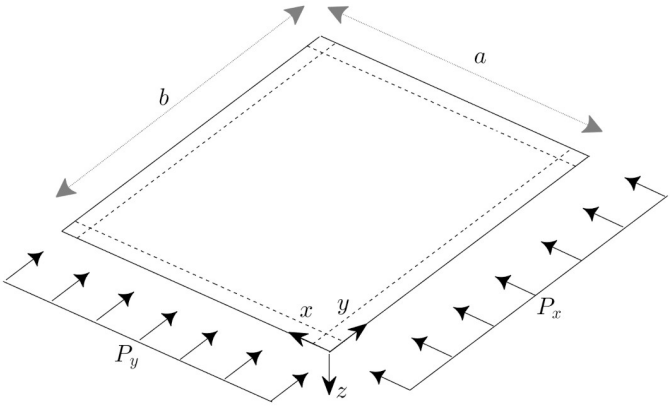

Fig. 1. Schematic of a plate under biaxial compression

where A, B, and D matrices are the familiar extensional, bending-extension coupling, and bending stiffnesses for composite materials, respectively, which can be calculated for a laminated composite with *nr* plies [27].

The equivalent form of equation (1) can be written as

$$\begin{bmatrix} \varepsilon^0 \\ \mathrm{M} \end{bmatrix} = \begin{bmatrix} \mathrm{A}^* & \mathrm{B}^* \\ \mathrm{B}^{**} & \mathrm{D}^* \end{bmatrix} \begin{bmatrix} \mathrm{N} \\ \kappa \end{bmatrix} \tag{2}$$

and $\mathrm{A}^* = \mathrm{A}^{-1}$, $\mathrm{B}^* = -\mathrm{A}^{-1}\mathrm{B}$, $\mathrm{B}^{**} = \mathrm{B}\mathrm{A}^{-1}$, and $\mathrm{D}^* = \mathrm{D} - \mathrm{B}\mathrm{A}^{-1}\mathrm{B}$. Other couplings (e.g. shear-extension and bend-twist) are out of the scope of the current study and it is assumed that the coefficients $A_{16} = A_{26} = D_{16} = D_{26} = 0$ are zero. One of the very practical layer arrangements with these conditions is antisymmetric cross-ply and/or angle-ply lamination.

The functions of stress $F(x, y)$ and deflection $w(x, y)$ can be substituted in the right-hand side of equation (2) by definition of $\mathrm{N}^T = \left(F_{,yy}\ F_{,xx}\ -F_{,xy}\right)$ and $\kappa^T = -\left(w_{,xx}\ w_{,yy}\ 2w_{,xy}\right)$, where a comma in subscript denotes a partial derivative. According to von Karman strains [28], the equilibrium equation is written as

$$\begin{aligned} &\frac{\partial^2 M_x}{\partial x^2} + \frac{\partial^2 M_y}{\partial y^2} + 2\frac{\partial^2 M_{xy}}{\partial x \partial y} + N_x\left(\frac{\partial^2 w}{\partial x^2} + \frac{\partial^2 \breve{w}}{\partial x^2}\right) \\ &\quad + N_y\left(\frac{\partial^2 w}{\partial y^2} + \frac{\partial^2 \breve{w}}{\partial y^2}\right) + 2N_{xy}\left(\frac{\partial^2 w}{\partial x \partial y} + \frac{\partial^2 \breve{w}}{\partial x \partial y}\right) = 0, \end{aligned} \tag{3}$$

and the compatibility equation is written as

$$\begin{aligned} &\frac{\partial^2 \varepsilon_x^0}{\partial y^2} + \frac{\partial^2 \varepsilon_y^0}{\partial x^2} - \frac{\partial^2 \varepsilon_{xy}^0}{\partial x \partial y} - \frac{\partial^2 w}{\partial x \partial y} \cdot \frac{\partial^2 w}{\partial x \partial y} + \frac{\partial^2 w}{\partial x^2} \cdot \frac{\partial^2 w}{\partial y^2} \\ &\quad + \frac{\partial^2 w}{\partial x^2} \cdot \frac{\partial^2 \breve{w}}{\partial y^2} + \frac{\partial^2 \breve{w}}{\partial x^2} \cdot \frac{\partial^2 w}{\partial y^2} - 2\frac{\partial^2 w}{\partial x \partial y} \cdot \frac{\partial^2 \breve{w}}{\partial x \partial y} = 0, \end{aligned} \tag{4}$$

and $\breve{w}$ is the initial geometrical imperfection of the plate. By substituting equation (2) into equations (3) and (4), one can rewrite these equations with respect to w and F as

$$a_1\left(\frac{\partial^4 F}{\partial x^2\partial y^2}\right)+a_2\left(\frac{\partial^4 w}{\partial x^2\partial y^2}\right)+a_3\left(\frac{\partial^4 F}{\partial x^4}\right)+a_4\left(\frac{\partial^4 F}{\partial y^4}\right)-a_5\left(\frac{\partial^4 w}{\partial x^4}\right)-a_6\left(\frac{\partial^4 w}{\partial y^4}\right)+\left(\frac{\partial^2 F}{\partial x^2}\right)\left(\frac{\partial^2 w}{\partial y^2}+\frac{\partial^2 \breve{w}}{\partial y^2}\right)-2\left(\frac{\partial^2 w}{\partial x\partial y}+\frac{\partial^2 \breve{w}}{\partial x\partial y}\right)\left(\frac{\partial^2 F}{\partial x\partial y}\right)+\left(\frac{\partial^2 F}{\partial y^2}\right)\left(\frac{\partial^2 w}{\partial x^2}+\frac{\partial^2 \breve{w}}{\partial x^2}\right)=0, \tag{5}$$

and

$$b_2\left(\frac{\partial^4 w}{\partial x^2\partial y^2}\right)+b_1\left(\frac{\partial^4 F}{\partial x^2\partial y^2}\right)+b_3\left(\frac{\partial^4 F}{\partial x^4}\right)+b_4\left(\frac{\partial^4 F}{\partial y^4}\right)-b_5\left(\frac{\partial^4 w}{\partial x^4}\right)-b_6\left(\frac{\partial^4 w}{\partial y^4}\right)+\left(\frac{\partial^2 w}{\partial y^2}+\frac{\partial^2 \breve{w}}{\partial y^2}\right)\left(\frac{\partial^2 w}{\partial x^2}\right)-\left(\frac{\partial^2 w}{\partial x\partial y}\right)^2-2\left(\frac{\partial^2 w}{\partial x\partial y}\right)\left(\frac{\partial^2 \breve{w}}{\partial x\partial y}\right)+\left(\frac{\partial^2 \breve{w}}{\partial x^2}\right)\left(\frac{\partial^2 w}{\partial y^2}\right)=0, \tag{6}$$

and unmentioned coefficients are listed in the Appendix.

2.1. Galerkin method

A familiar and fast analytical solution of equations (5) and (6) is based on the Galerkin method. Due to simply supported boundary conditions, the deflection and geometrical imperfection can be chosen in the form of sinusoidal function as

$$\begin{aligned} w &= f\sin(m_1 x)\sin(n_1 y),\\ \breve{w} &= g\sin(m_1 x)\sin(n_1 y),\\ m_1 &= \frac{\bar{m}\pi}{a},\quad n_1=\frac{\bar{n}\pi}{b}, \end{aligned} \tag{7}$$

where f is an unknown amplitude of deflection, and g is a known amplitude of geometrical imperfection, and $\bar{m}$ and $\bar{n}$ are the number of half waves in directions x and y. By substituting equation (7) in equation (6), the stress function can be derived analytically as

$$F=\psi_1\cos(2m_1x)+\psi_2\cos(2n_1y)+\psi_3\sin(m_1x)\sin(n_1y)-0.5P_x hy^2-0.5P_y hx^2, \tag{8a}$$

where

$$\psi_1=\frac{f(f+2g)n_1^2}{32b_3m_1^2},\quad \psi_2=\frac{f(f+2g)m_1^2}{32b_4n_1^2},\quad \psi_3=-\frac{f\left(b_2m_1^2n_1^2-b_5m_1^4-b_6n_1^4\right)}{b_1m_1^2n_1^2+b_3m_1^4+b_4n_1^4}. \tag{8b}$$

To solve the equilibrium equation (5), the assumed deflection in equation (7) and the stress function in equation (8a) are substituted in equation (5). Since the deflection is only an assumption, these substitutions do not lead to satisfaction in equation (5) and they result in a residual. Then, the Galerkin integral can be written as [29, 30]

$$\int_0^b\int_0^a \text{residual}\cdot\sin(m_1x)\sin(n_1y)\,\mathrm{d}x\,\mathrm{d}y=0. \tag{9}$$

By integrating, simplifying, and neglecting small values, the result can be obtained as

$$f+\frac{P_x}{P_{cr}}(f+g)+c_1f^3+c_2f^2=0, \tag{10a}$$

where the buckling load P_{cr} and other coefficients are listed in the Appendix. Equation (10a) is a closed-form relationship between load P_x and deflection f. It should be noted that the value of c_2 is exceedingly small and negligible. Then, for the perfect plates ($g=0$), equation (10a) can be rewritten as

$$\frac{P_x}{P_{cr}}=1+c_1f^2. \tag{10b}$$

It is a parabolic relation between P_x/P_{cr} and f. In other words, there will be a bifurcation in the equilibrium path. In addition, the results of previous investigations [17–26] indicate that there is a bifurcation-type equilibrium path for the case of perfect plates. However, the results of other numerical methods like the finite element method [12, 13] are contrary and their results may have a non-bifurcation equilibrium path for some cases of non-zero coupling matrix. Then, the authors of the current study tried to find the conflict between different methods and understand when the coupling matrix leads to non-zero deflection before buckling.

It is found that it is vital to satisfy the boundary condition. In other words, when the EB coupling matrix is non-zero, some boundary conditions are not satisfied in previous work [17–26]. For simply supported edges, the following essential conditions should be satisfied [31]

$$\begin{aligned} &x=0,\ a:\ w=0,\ N_x=-P_xh,\ N_{xy}=0,\ M_x=0,\\ &y=0,\ b:\ w=0,\ N_y=-P_yh,\ N_{xy}=0,\ M_y=0, \end{aligned} \tag{11}$$

where deflection w is zero at all edges due to defining a sinusoidal function in equation (7). The force resultants N_x, N_y, and N_{xy} are satisfied as a weak form condition (or integral form) [31]. However, the moment resultants M_x and M_y are non-zero due to the existence of the EB coupling matrix. This is the main reason for contradictory results in the literature review. To scrutinize this lack, equation (2) can be rewritten in detail as

$$\begin{aligned} M_x &= B_{11}^{**}F_{,yy}+B_{12}^{**}F_{,xx}-B_{16}^{**}F_{,xy}-D_{11}^{*}w_{,xx}+D_{12}^{*}w_{,yy},\\ M_y &= B_{21}^{**}F_{,yy}+B_{22}^{**}F_{,xx}-B_{26}^{**}F_{,xy}-D_{21}^{*}w_{,xx}+D_{22}^{*}w_{,yy}, \end{aligned} \tag{12a}$$

where their values at the edges are

$$M_x = -B_{11}^{**}P_x h - B_{12}^{**}P_y h \neq 0,$$
$$M_y = -B_{21}^{**}P_x h - B_{22}^{**}P_y h \neq 0. \tag{12b}$$

To overcome this problem, it can be assumed that four rotational springs are distributed along four edges of the plate. Therefore, the right-hand side of equation (12b) should equal

$$\begin{aligned}
M_x\Big|_{x=0} &= -B_{11}^{**}P_x h - B_{12}^{**}P_y h = -K_1\left(\frac{\partial w}{\partial x}\right)_{x=0},\\
M_x\Big|_{x=a} &= -B_{11}^{**}P_x h - B_{12}^{**}P_y h = +K_1\left(\frac{\partial w}{\partial x}\right)_{x=a},\\
M_y\Big|_{y=0} &= -B_{21}^{**}P_x h - B_{22}^{**}P_y h = -K_2\left(\frac{\partial w}{\partial y}\right)_{y=0},\\
M_y\Big|_{y=b} &= -B_{21}^{**}P_x h - B_{22}^{**}P_y h = +K_2\left(\frac{\partial w}{\partial y}\right)_{y=b}.
\end{aligned} \tag{12c}$$

However, due to the assumption of the artificial springs at the edges, the equilibrium equation will be changed.

2.2. Virtual displacement principle

To derive the equilibrium equation of the plate surrounded by the springs, the virtual displacement principle can be applied, where a variation of total potential energy $\delta\Pi$ is equal to the subtraction of the variation of internal strain energy δU and the variation of external loads δW (i.e. $\delta\Pi = \delta U - \delta W = 0$). The variation of internal strain energy can be written as integral form as

$$\delta U = \int_0^b\int_0^a \Big[N_x\delta\varepsilon_x^0 + N_y\delta\varepsilon_y^0 + N_{xy}\delta\varepsilon_{xy}^0 + M_x\delta\kappa_x + M_y\delta\kappa_y + M_{xy}\delta\kappa_{xy}\Big]\,\mathrm{d}x\,\mathrm{d}y. \tag{13a}$$

By employing classical theory and von Karman non-linear relationships, the final form of equation (13a) can be obtained as

$$\begin{aligned}
\delta U = \int_0^b\int_0^a \Bigg[&\frac{\partial^2 M_x}{\partial x^2} + \frac{\partial^2 M_y}{\partial y^2} + 2\frac{\partial^2 M_{xy}}{\partial x\partial y}\\
&+ N_x\left(\frac{\partial^2 w}{\partial x^2} + \frac{\partial^2 \breve{w}}{\partial x^2}\right) + N_y\left(\frac{\partial^2 w}{\partial y^2} + \frac{\partial^2 \breve{w}}{\partial y^2}\right)\\
&+ 2N_{xy}\left(\frac{\partial^2 w}{\partial x\partial y} + \frac{\partial^2 \breve{w}}{\partial x\partial y}\right)\Bigg]\delta w\,\mathrm{d}x\,\mathrm{d}y.
\end{aligned} \tag{13b}$$

The inside of the above multiple integral is equal to the equilibrium equation in equation (3). The variation of external loads due to in-plane compression can be calculated as

$$\delta W = \int_0^b \Big[-P_x(\delta u)\Big]_{x=0}^{x=a}\mathrm{d}y + \int_0^a \Big[-P_y(\delta v)\Big]_{y=0}^{y=b}\mathrm{d}x, \tag{14a}$$

where (u, v) are in-plane displacements. The variation of external loads due to moments of artificial springs can be calculated as

$$\delta W = -\int_0^b \left[M_x\left(\frac{\partial w}{\partial x}\right)\right]_{x=0}^{x=a}\mathrm{d}y - \int_0^a \left[M_y\left(\frac{\partial w}{\partial y}\right)\right]_{y=0}^{y=b}\mathrm{d}x. \tag{14b}$$

Therefore, by employing recent equations, the variation of total potential energy will be equal to

$$\begin{aligned}
&\int_0^b\int_0^a \Bigg[\frac{\partial^2 M_x}{\partial x^2} + \frac{\partial^2 M_y}{\partial y^2} + 2\frac{\partial^2 M_{xy}}{\partial x\partial y}\\
&\quad + N_x\left(\frac{\partial^2 w}{\partial x^2} + \frac{\partial^2 \breve{w}}{\partial x^2}\right) + N_y\left(\frac{\partial^2 w}{\partial y^2} + \frac{\partial^2 \breve{w}}{\partial y^2}\right)\\
&\quad + 2N_{xy}\left(\frac{\partial^2 w}{\partial x\partial y} + \frac{\partial^2 \breve{w}}{\partial x\partial y}\right)\Bigg]\delta w\,\mathrm{d}x\,\mathrm{d}y\\
&\quad - \left(B_{11}^{**}P_x h + B_{12}^{**}P_y h\right)\int_0^b \left[\frac{\partial w}{\partial x}\right]_{x=0}^{x=a}\mathrm{d}y\\
&\quad - \left(B_{21}^{**}P_x h + B_{22}^{**}P_y h\right)\int_0^a \left[\frac{\partial w}{\partial y}\right]_{y=0}^{y=b}\mathrm{d}x = 0.
\end{aligned} \tag{15}$$

Again, by integrating, simplifying, and neglecting small values, the result can be obtained as

$$f + \frac{P_x}{P_{cr}}(f + g + r) + c_1 f^3 + c_2 f^2 = 0. \tag{16}$$

The only difference between equation (10a) and equation (16) is in coefficient r which is defined as $r = k_6/k_3$, and

$$\begin{aligned}
k_3 &= \frac{h\pi^2\left(Ra^2\bar{n}^2 + b^2\bar{m}^2\right)}{4ba},\\
k_6 &= \frac{h\left(RB_{12}^{**} + B_{11}^{**}\right)\bar{m}b\begin{pmatrix}-(-1)^{\bar{m}}+1\\ +(-1)^{\bar{m}+\bar{n}} - (-1)^{\bar{n}}\end{pmatrix}}{a\bar{n}}\\
&\quad + \frac{h\left(RB_{22}^{**} + B_{21}^{**}\right)\bar{n}a\begin{pmatrix}-(-1)^{\bar{m}}+1\\ +(-1)^{\bar{m}+\bar{n}} - (-1)^{\bar{n}}\end{pmatrix}}{b\bar{m}}.
\end{aligned} \tag{17}$$

It should be noted that the effect of the coefficient r in equation (16) is like the effect of geometrical imperfection g. So, this novel parameter is called the EB coupling imperfection in the next section, and it is useful to compare with respect to the geometrical imperfection. According to equation (17), the EB coupling imperfection can be calculated for different types of composites (e.g. FGM) using their familiar A, B, and D matrices. However, it is presented only for GFRP laminated composites in this study.

2.3. Virtual displacement principle for non-square plates

For the case of square GFRP laminated composite plates, there will be a one-half wave in both x and y directions ($\bar{m} = \bar{n} = 1$).

Therefore, equation (17) can be simplified as

$$r = \frac{16}{\pi^2}\left(B_{11}^{**} + B_{21}^{**}\right). \tag{18}$$

The results of an extensive finite element analysis in ANSYS show that the deflection function in equation (7) is not suitable for the case of non-square ($a/b > 1.5$) and unsymmetric plates and there will be a mixed-mode response. The term "mixed mode" was recently introduced in [32] for the first time in the literature for far equilibrium path and dynamic response of isotropic plates. However, this phenomenon will be demonstrated in the next section for the case of non-square and unsymmetric laminated plates. In other words, the EB coupling imperfection leads to a mode shape $\bar{m} = \bar{n} = 1$ and the geometry yields another mode. For instance, the mixed mode of a plate with $a/b = 3$ is illustrated in Fig. 2. The deflection has two modes as $(\bar{m} = \bar{n} = 1)$ and $(\bar{m} = 3, \bar{n} = 1)$. Therefore, a proper deflection function is

$$w = f_1 \sin\left(\frac{\pi}{a}x\right)\sin\left(\frac{\pi}{b}y\right) + f_2 \sin\left(\frac{3\pi}{a}x\right)\sin\left(\frac{\pi}{b}y\right) \tag{19}$$

or equivalently for two pairs of arbitrary mode shapes

$$w = f_1 \sin(m_1 x)\sin(n_1 y) + f_2 \sin(m_2 x)\sin(n_2 y) \tag{20}$$

and

$$\breve{w} = g_1 \sin(m_1 x)\sin(n_1 y) + g_2 \sin(m_2 x)\sin(n_2 y), \tag{21}$$

where

$$m_1 = \frac{\bar{m}_1\pi}{a}, \quad n_1 = \frac{\bar{n}_1\pi}{b}, \quad m_2 = \frac{\bar{m}_2\pi}{a}, \quad n_2 = \frac{\bar{n}_2\pi}{b}. \tag{22}$$

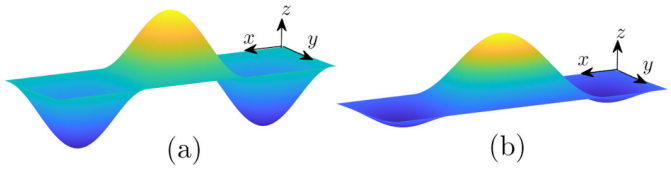

Fig. 2. The effect of mixed mode for a plate with $\frac{a}{b} = 3$, (a) the single mode from equation (5) and (b) the mixed mode from equation (19) when $f_1 \cdot f_2 < 0$

By substituting equations (20) and (21) into equation (6), the stress function can be derived analytically. However, due to limitations in pages, it is not mentioned here. Then, the stress and deflection functions can be substituted in the variation of total potential energy in equation (15). By integrating and simplifying, the results can be derived in two equilibrium equations for finding f_1 and f_2. However, the general solution will have huge terms, and due to limitations in pages, a case study $(\bar{m}_1 = \bar{n}_1 = \bar{n}_2 = 1, \bar{m}_2 = 3)$ is listed here as

$$\begin{aligned}
&f_1 + \frac{P_x}{P_{cr1}}(f_1 + g_1 + r_1) \\
&\quad + \frac{1}{h_4}\left(h_1 f_1^2 + h_2 f_2^2 + h_3 f_1 f_2 + h_5 f_2\right. \\
&\quad + h_7 f_1^3 + h_8 f_2^3 + h_9 f_1^2 f_2 + h_{10} f_1 f_2^2 \\
&\quad \left. + h_{11} f_1^2 + h_{12} f_2^2 + h_{13} f_1 f_2\right) = 0, \\
&f_2 + \frac{P_x}{P_{cr2}}(f_2 + g_2 + r_2) \\
&\quad + \frac{1}{h_{18}}\left(h_{14} f_1^2 + h_{15} f_2^2 + h_{16} f_1 f_2 + h_{17} f_1\right. \\
&\quad + h_{20} f_1^3 + h_{21} f_2^3 + h_{22} f_1^2 f_2 + h_{23} f_1 f_2^2 \\
&\quad \left. + h_{24} f_1^2 + h_{25} f_2^2 + h_{26} f_1 f_2\right) = 0,
\end{aligned} \tag{23}$$

where

$$P_{cr1} = \frac{h_4}{h_6}, \quad r_1 = \frac{h_{27}}{h_6}, \quad P_{cr2} = \frac{h_{18}}{h_{19}}, \quad r_2 = \frac{h_{28}}{h_{19}}, \tag{24}$$

and the coefficients $h_1, \ldots, h_{28}$ are some explicit functions that can be provided at the request of the readers. As expected, there are two types of EB coupling imperfections as r_1 and r_2 and two geometrical imperfections as g_1 and g_2 in equation (23) which are related to two mode shapes of mixed response.

3. NUMERICAL EXAMPLES

To illustrate the effect of EB coupling matrix on bifurcation-type and/or non-bifurcation-type equilibrium paths of the laminated composite plates, a lamina made of GFRP [33] with the following material properties is considered: $E_1 = 40$ GPa, $E_2 = E_3 = 9$ GPa, $G_{12} = G_{31} = 3.4$ GPa, $G_{23} = 2.7$ GPa and $\nu_{12} = 0.28$. Then, the matrices A, B, and D can be calculated for different types of lay-up sequences [27]. Again, it is repeated that the shear-extension and bend-twist couplings are out of scope, and it is assumed that the coefficients $A_{16} = A_{26} = D_{16} = D_{26} = 0$ are zero. Therefore, a familiar example is the antisymmetric lay-up sequence, which can be used in different cross-ply and/or angle-ply cases. The geometrical parameters of different types of examples (e.g. square, and rectangular) are $a = b = 100$ mm, $a = 2b = 200$ mm, and $a = 3b = 300$ mm, and the thickness is $h = 1$ mm. In all cases, the current results are compared with the FEM results of ANSYS software (see [34] for element type). In the figures, the variation of dimensionless load P/P_{cr} versus dimensionless deflection $w_{\max}/h$ or w_c/h are plotted, where $w_{\max}$ denotes the maximum deflection of the plate and w_c is the deflection corresponding to the center of the plate. The calculation of P_{cr} in non-bifurcation cases are not sensible. It should be noted that the calculation of this parameter in ANSYS is based on linear buckling analysis [34]. In the present study, it is calculated from the explicit equation in the Appendix for single mode and from equation (24) for mixed mode. Since the in-plane displacements at edges remain straight in the post-buckling range [31], this condition is provided by the coupling boundary condition in ANSYS.

The results of solutions of equations (10a) and (16) are compared in Fig. 3, for a square laminated composite plate

$[(0/90)_4]_T$ under uniaxial compression ($R = 0$). The geometrical imperfection amplitude g/h is equal to 0.001. As seen, without considering the mentioned boundary condition in equation (12c), the equilibrium path tends to have bifurcation-type buckling (when $g/h \to 0$). On the other hand, the effect of such a boundary condition is like adding another imperfection, which is called the EB coupling imperfection (r) in the present study. However, the value is negative in this case. Therefore, the deflection grows in the opposite side ($-z$). According to comparisons with FEM results, satisfying all boundaries is of great significance to get reliable results.

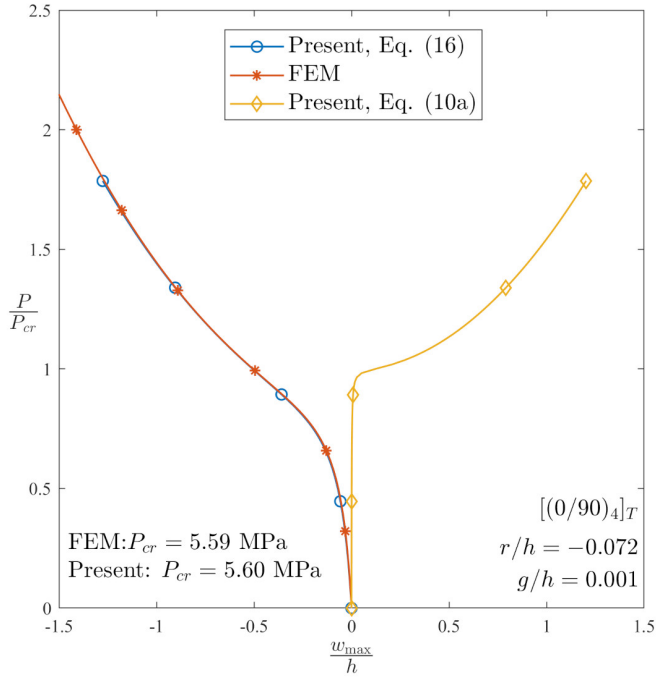

Fig. 3. Equilibrium path of a plate with and without satisfying proper boundary condition

According to equation (12b), when a plate is subjected to uniaxial compression, only B_{11}^{**} and B_{21}^{**} have influence on the value of coupling imperfection. However, a plate under biaxial compression has more complexity due to the existence of B_{11}^{**}, B_{21}^{**}, B_{12}^{**}, and B_{22}^{**}. This effect is shown in Fig. 4 for a square laminated composite plate $[(90/0)_4]_T$ with a geometrical imperfection of 0.001. Unexpectedly, the biaxial loading does not make EB imperfection in the equilibrium path. Because the antisymmetric cross-ply laminate has $B_{11}^{**} = -B_{22}^{**}$ and $B_{12}^{**} = -B_{21}^{**}$. According to the Appendix and equation (17), r has zero value for $R = 1$. Indeed, for other non-symmetric cases or different loading ratio ($R \neq 1$), there will be non-zero r. It is expected that the perfect plate $[(90/0)_4]_T$ under equally biaxial compression has exactly a bifurcation-type equilibrium path.

There are two other points which can be found in Fig. 4. First, by comparing Fig. 3 (blue line) and Fig. 4 (blue line), it can be found that $[(0/90)_4]_T$ and $[(90/0)_4]_T$ have negative and positive deflection growth, respectively. Because the value of EB coupling imperfection is equal, it has a different sign, and this sign is highly dependent on the lay-up sequence. Second,

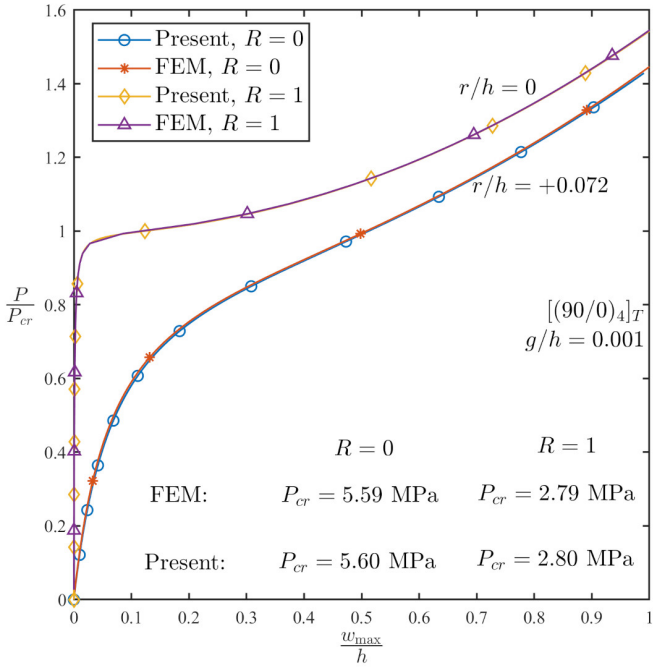

Fig. 4. Equilibrium path of a plate under uniaxial/biaxial compression

for a plate under shear load (not presented here), also B_{16}^{**} and B_{26}^{**} will influence the value of EB coupling imperfection.

In Fig. 5, four different antisymmetric cross-ply laminated composite square plates $[(90/0)_{nr}]_T$ are investigated, where $nr = 2, 4, 8, 16$, and the total thickness is the same. In all cases of this example, the plate with zero value of geometrical imperfection is subjected to uniaxial compression. As can be seen, alternatively, by increasing the number of 0- and 90-degree plies, the magnitude of coefficients of the coupling matrix (or equiva-

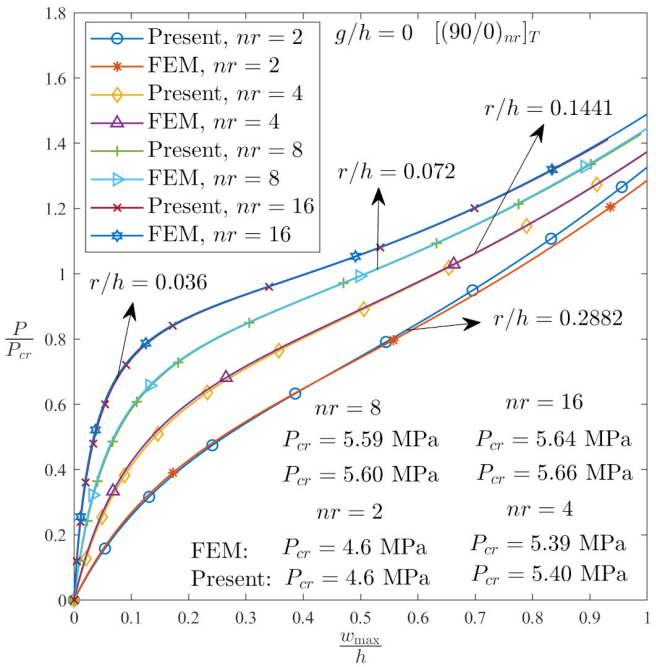

Fig. 5. Equilibrium path of a plate with different number of plies

lently B**) are reduced. Subsequently, the last curves ($nr = 16$) are getting to be close to the bifurcation-type equilibrium path. As seen, the coefficient r is useful to demonstrate the amount of EB coupling as a quantity.

One of the important case studies can be seen in the plates with antisymmetric angle-ply lay-up sequences where non-zero coefficients of B** are B^{**}_{16}, B^{**}_{26}, B^{**}_{61}, and B^{**}_{62}. However, these coefficients are zero for cross-ply and other remaining coefficients of B** are non-zero (i.e. B^{**}_{11}, B^{**}_{12}, B^{**}_{21}, and B^{**}_{22}). As explained before, B^{**}_{16} and B^{**}_{26} are significant for the plates under shear load. Also, B^{**}_{61} and B^{**}_{62} have no effect in the amount of EB coupling imperfection according to equation (17). To verify this report, different types of antisymmetric angle-ply lay-up sequences (e.g. $[(15/-15)_4]_T$, $[(30/-30)_4]_T$, and $[(45/-45)_4]_T$) are selected and their results are illustrated in Fig. 6. For convenience, the lay-up sequence can be demonstrated as $[(\theta/-\theta)_4]_T$, which $\theta = 15, 30, 45$. The geometrical imperfection of the square plate is 0.001 and the plate is subjected to uniaxial compression. As expected, both ANSYS and present results show that all antisymmetric angle-ply cases tend to have bifurcation points when $g/h \to 0$.

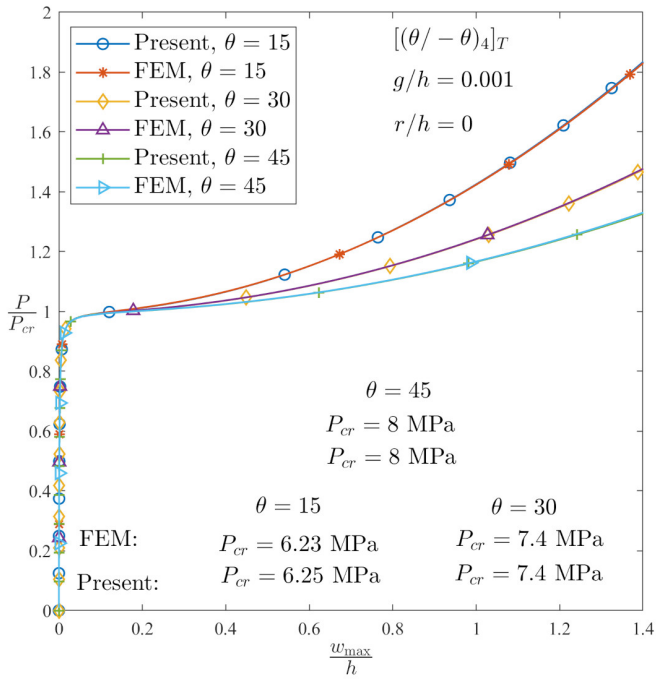

Fig. 6. Equilibrium path of a plate with different angle-ply cases

In all the above examples, there was a unique half wave in x and y directions (i.e. $\bar{m} = \bar{n} = 1$). According to the definition of coupling imperfection r (see the Appendix), it is highly dependent on the number of half waves. It can be observed that for an even number of half waves, it will be zero. Then, a question can arise if there is a bifurcation-type equilibrium path for a rectangular plate with $a/b = 2$. To investigate this case, three different cases of aspect ratio are considered, and the results are shown in Fig. 7a. In this problem, the laminated composite plate $[(90/0)_4]_T$ with zero geometrical imperfection is subjected to uniaxial compression. An interesting point can be seen in the case of $a/b = 2$, in which the plate tends to have three half waves ($\bar{m} = 3$). However, the eigenvalue buckling mode shape is $\bar{m} = 2$. Because the plate cannot ignore the existence of the EB coupling imperfection. Therefore, a novel finding of the current paper is that there are some possibilities to have different mode shapes in linear and non-linear buckling analysis. Another significant finding is that the EB coupling imperfection has a mode

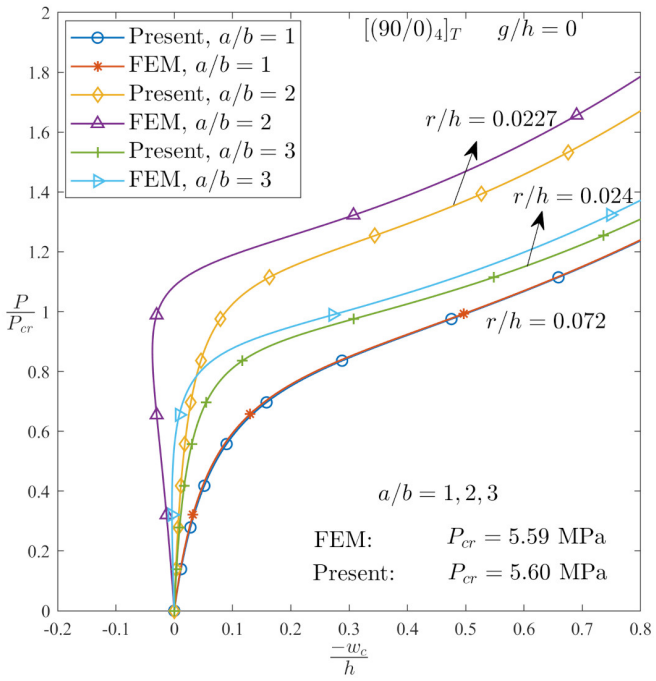

(a)

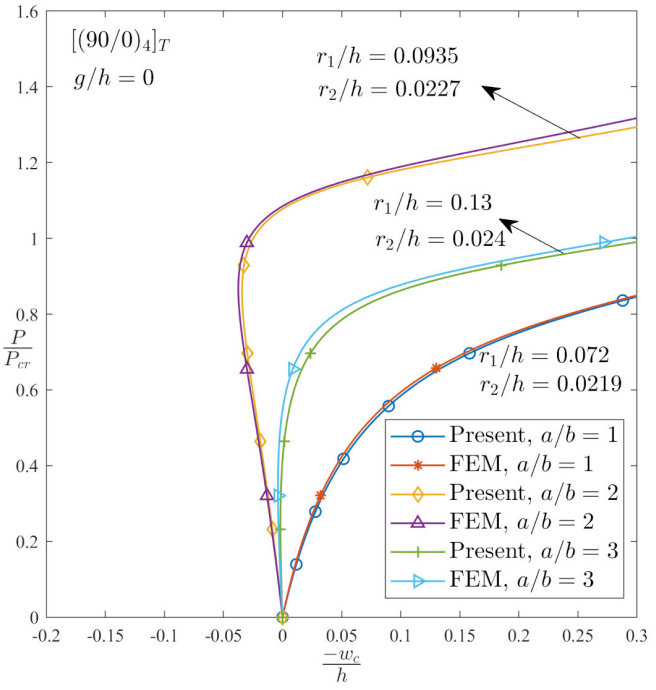

(b)

Fig. 7. Equilibrium path of a plate with considering different aspect ratio by employing (a) equation (16) and (b) equation (23)

shape like $\bar{m} = \bar{n} = 1$. When a plate has a non-square geometry, the deflection will be mixed into two modes (in these cases, $\bar{m} = \bar{n} = 1$ and $\bar{m} = 3$, $\bar{n} = 1$). Therefore, the assumed deflection with a single mode (see equation (7)) is not enough to give more accurate results. Therefore, the results of the deflection with simultaneous two modes in equation (23) are compared in Fig. 7b and a good agreement can be seen between the two methods of solution.

In the presence of the EB coupling matrix, many other effects cause bifurcation-type or non-bifurcation-type equilibrium paths. For instance, it is proved that the main reason for non-bifurcation is the simply supported boundary condition (see equation (11)). Therefore, it is expected that for clamped conditions, the plate gives a bifurcation-type equilibrium path. Due to the assumed deflection function (see equation (7)) not being suitable for this boundary condition, only the results of ANSYS are shown in Fig. 8. As seen, the clamped square plate $[(90/0)_4]_T$ with the geometrical imperfection of 0.001 is not affected by EB coupling matrix and beyond the buckling load the deflection grows relatively suddenly.

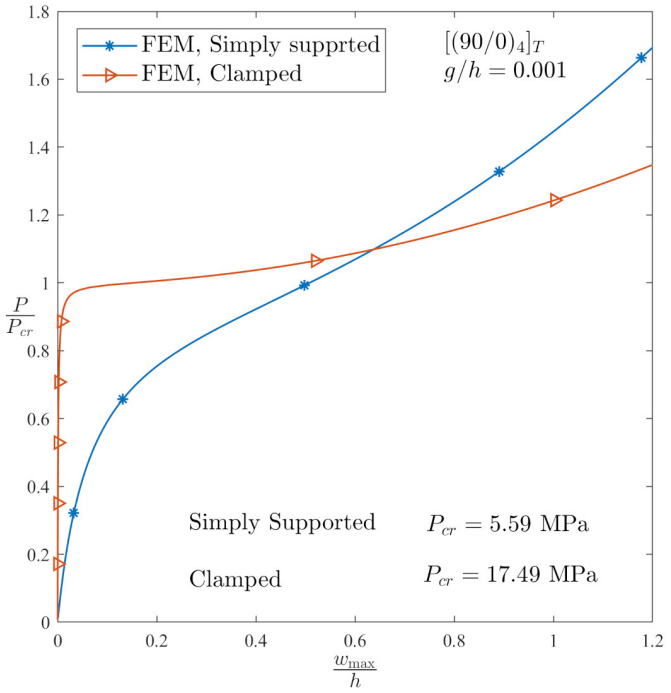

Fig. 8. Equilibrium paths with simply supported or clamped edges

4. CONCLUSIONS

First, the equilibrium and compatibility equations of laminated composite plates are solved by an analytical Galerkin method, and a closed-form solution of loading and deflection of the plate is derived. It is explained that in the presence of the EB coupling matrix, the essential boundary conditions will be changed. By assuming an artificial rotational spring, the boundary conditions are satisfied. Second, the equilibrium equation is modified by additional terms in the virtual displacement principle. Third, the deflection function was changed to cover non-square plates. As a reflection of the prospect, such analytical formulations can be employed to investigate whether the concept of bifurcation buckling applies to unsymmetric laminated composite plates. In the numerical results, it is demonstrated that satisfying all boundaries is of great significance to obtain reliable results. It is shown the existence of a coupling matrix does not always mean giving a non-bifurcation-type equilibrium path and the value (EB coupling imperfection) depends on:

Load: One of the influencing factors is the type of load. In the case of uniaxial load, B^{**}_{11}, B^{**}_{21} lead to the coupling imperfection. In the case of biaxial load, all B^{**}_{11}, B^{**}_{12}, B^{**}_{21}, B^{**}_{22} influence the coupling imperfection. In the case of shear load, only B^{**}_{16}, B^{**}_{26} make a condition for non-bifurcation.

Number of plies: By increasing the number of plies, the magnitude of coefficients of B^{**} decreases. This reduction makes the equilibrium path of the plates closer to the bifurcation-type one.

Antisymmetric angle-ply: This lay-up sequence has a non-zero coupling matrix only in B^{**}_{16}, B^{**}_{26}, B^{**}_{61}, B^{**}_{62}. None of these coefficients affects the coupling imperfection.

Rectangular Plate: The EB coupling matrix may change the mode shape of the rectangular plate in the post-buckling regime, in which the number of half waves will be odd. However, it can be an even number in eigenvalue buckling analysis. Also, the mode shape will be a mix of first ($m = n = 1$) and a mode shape with odd numbers with the lowest buckling load.

Clamped: In the case of a clamped boundary condition, there is no effect of the coupling matrix on the non-bifurcation type of the equilibrium path.

APPENDIX

The coefficients in equation (6), (8a), and (16) are defined as

$$a_1 = B^{**}_{11} + B^{**}_{22} - 2B^{**}_{66}, \quad a_2 = -D^{*}_{12} - D^{*}_{21} - 4D^{*}_{66},$$
$$a_3 = B^{**}_{12}, \quad a_4 = B^{**}_{21}, \quad a_5 = D^{*}_{11}, \quad a_6 = D^{*}_{22},$$
$$b_1 = 2A^{*}_{12} + A^{*}_{66}, \quad b_2 = -B^{*}_{22} + 2B^{*}_{66} - B^{*}_{11},$$
$$b_3 = A^{*}_{22}, \quad b_4 = A^{*}_{11}, \quad b_5 = B^{*}_{21}, \quad b_6 = B^{*}_{12},$$
$$P_{cr} = \left(\frac{k_3}{k_2}\right)^{-1}, \quad c_1 = \frac{k_4}{k_2}, \quad c_2 = \frac{k_1}{k_2} + \frac{k_5}{k_2},$$
$$k_1 = \frac{\pi^2 mn\,(a_3 b_4 + a_4 b_3)\,((-1)^m - 1 - (-1)^{m+n} + (-1)^n)}{6ba b_3 b_4},$$
$$k_2 = -\frac{\pi^4 \begin{pmatrix} n^8\,(-a_4 b_6 + a_6 b_4)\,a^8 \\ +n^6 b^2 m^2\,(-a_1 b_6 - a_2 b_4 + a_4 b_2 + a_6 b_1)\,a^6 \\ +b^4 m^4 n^4 \begin{pmatrix} a_1 b_2 - a_2 b_1 - a_3 b_6 \\ -a_4 b_5 + a_5 b_4 + a_6 b_3 \end{pmatrix} a^4 \\ +b^6 m^6 n^2 \begin{pmatrix} -a_1 b_5 - a_2 b_3 \\ +a_3 b_2 + a_5 b_1 \end{pmatrix} a^2 \\ +b^8 m^8\,(-a_3 b_5 + a_5 b_3) \end{pmatrix}}{4a^3 b^3\left(a^4 b_4 n^4 + a^2 b^2 b_1 m^2 n^2 + b^4 b_3 m^4\right)},$$

$$k_3 = \frac{h\pi^2\left(Ra^2n^2+b^2m^2\right)}{4ba}, \quad k_4 = -\frac{\pi^4\left(a^4b_4n^4+b^4b_3m^4\right)}{64b^3a^3b_3b_4},$$

$$k_5 = \frac{2n\begin{pmatrix} a^4b_6n^4 \\ -a^2b^2b_2m^2n^2 \\ +b^4b_5m^4 \end{pmatrix} m\pi^2\left(-1+(-1)^m\right)\left((-1)^n-1\right)}{3ba\left(a^4b_4n^4+a^2b^2b_1m^2n^2+b^4b_3m^4\right)},$$

$$k_6 = \frac{h\left(RB_{12}^{**}+B_{11}^{**}\right)mb\begin{pmatrix} -(-1)^m+1 \\ +(-1)^{m+n}-(-1)^n \end{pmatrix}}{an} + \frac{h\left(RB_{22}^{**}+B_{21}^{**}\right)na\begin{pmatrix} -(-1)^m+1 \\ +(-1)^{m+n}-(-1)^n \end{pmatrix}}{bm}.$$

ACKNOWLEDGEMENTS

This work has been supported by the Polish National Science Centre (NCN) under the project OPUS 17 No. 2019/33/B/ST8/00182.

REFERENCES

[1] N. Vasiraja and P. Nagaraj, "The effect of material gradient on the static and dynamic response of layered functionally graded material plate using finite element method," *Bull. Pol. Acad. Sci. Tech. Sci.*, vol. 67, no. 4, pp. 827–838, 2019, doi: 10.24425/bpasts.2019.130191.

[2] D. Van Dung and N.T. Nga, "Buckling and postbuckling nonlinear analysis of imperfect FGM plates reinforced by FGM stiffeners with temperature-dependent properties based on TSDT," *Acta Mech.*, vol. 227, pp. 2377–2401, 2016, doi: 10.1007/s00707-016-1637-y.

[3] Z. Kolakowski and R.J. Mania, "Influence of the coupling matrix B on the interactive buckling of FML-FGM columns with closed cross-sections under axial compression," *Compos. Struct.*, vol. 173, pp. 70–77, 2017, doi: 10.1016/j.compstruct.2017.03.108.

[4] M. Mikuśkiewicz, "Silicon nitride/carbon nanotube composites: preparation and characterization," *Bull. Pol. Acad. Sci. Tech. Sci.*, vol. 69, no. 5, e138234, 2021, doi: 10.24425/bpasts.2021.138234.

[5] E.A. Pieczyska, S.P. Gadaj, W.K. Nowacki, and H. Tobushi, "Thermomechanical investigations of martensitic and reverse transformations in TiNi shape memory alloy," *Bull. Pol. Acad. Sci. Tech. Sci.*, vol. 52, no. 3, pp. 165–171, 2004.

[6] K. Asemi and M. Shariyat, "Three-dimensional biaxial postbuckling analysis of heterogeneous auxetic rectangular plates on elastic foundations by new criteria," *Comput. Methods. Appl. Mech. Eng.*, vol. 302, pp. 1–26, 2016, doi: 10.1016/j.cma.2015.12.026.

[7] Y.X. Hao, W. Zhang, and J. Yang, "Nonlinear oscillation of a cantilever FGM rectangular plate based on third-order plate theory and asymptotic perturbation method," *Compos. B. Eng.*, vol. 42, no. 3, pp. 402–413, 2011, doi: 10.1016/j.compositesb.2010.12.010.

[8] J.J. Mao and W. Zhang, "Buckling and post-buckling analyses of functionally graded graphene reinforced piezoelectric plate subjected to electric potential and axial forces," *Compos. Struct.*, vol. 216, pp. 392–405, 2019, doi: 10.1016/j.compstruct.2019.02.095.

[9] A. Wang, H. Chen, Y. Hao, and W. Zhang, "Vibration and bending behavior of functionally graded nanocomposite doubly-curved shallow shells reinforced by graphene nanoplatelets," *Results Phys.*, vol. 9, pp. 550–559, 2018, doi: 10.1016/j.rinp.2018.02.062.

[10] J.J. Mao and W. Zhang, "Linear and nonlinear free and forced vibrations of graphene reinforced piezoelectric composite plate under external voltage excitation," *Compos. Struct.*, vol. 203, pp. 551–565, 2018, doi: 10.1016/j.compstruct.2018.06.076.

[11] Y. Wang and W. Zhang, "On the thermal buckling and post-buckling responses of temperature-dependent graphene platelets reinforced porous nanocomposite beams," *Compos. Struct.*, vol. 296, pp. 115880, 2022, doi: 10.1016/j.compstruct.2022.115880.

[12] E. Carrera, R. Azzara, E. Daneshkhah, A. Pagani, and B. Wu, "Buckling and post-buckling of anisotropic flat panels subjected to axial and shear in-plane loadings accounting for classical and refined structural and nonlinear theories," *Int. J. Nonlinear Mech.*, vol. 133, 103716, 2021, doi: 10.1016/j.ijnonlinmec.2021.103716.

[13] H.R. Ovesy, S.A.M. GhannadPour and G. Morada, "Post-buckling behavior of composite laminated plates under end shortening and pressure loading, using two versions of finite strip method," *Compos. Struct.*, vol. 75, pp. 106–113, 2006, doi: .

[14] Z. Kolakowski and R.J. Mania, "Dynamic response of thin FG plates with a static unsymmetrical stable postbuckling path," *Thin-Walled Struct.*, vol. 86, pp. 10–17, 2015, doi: 10.1016/ j.tws.2014.09.004.

[15] A. Lal, K.R. Jagtap, and B.N. Singh, "Post buckling response of functionally graded materials plate subjected to mechanical and thermal loadings with random material properties," *Appl. Math. Model.*, vol. 37, no. 5, pp. 2900–2920, 2013, doi: 10.1016/j.apm.2012.06.013.

[16] D.G. Zhang, "Thermal post-buckling and nonlinear vibration analysis of FGM beams based on physical neutral surface and high order shear deformation theory," *Meccanica*, vol. 49, pp. 283–293, 2014, doi: 10.1007/s11012-013-9793-9.

[17] H. Huang and Q. Han. "Nonlinear elastic buckling and post-buckling of axially compressed functionally graded cylindrical shells," *Int. J. Mech. Sci.*, vol. 51, no. 7, pp. 500–507, 2009, doi: 10.1016/j.ijmecsci.2009.05.002.

[18] H. Huang and Q. Han, "Nonlinear dynamic buckling of functionally graded cylindrical shells subjected to time-dependent axial load," *Compos. Struct.*, vol. 92, no. 2, pp. 593–598, 2010, doi: 10.1016/j.compstruct.2009.09.011.

[19] N.D. Duc and P.H. Cong. "Nonlinear postbuckling of an eccentrically stiffened thin FGM plate resting on elastic foundations in thermal environments," *Thin-Walled Struct.*, vol. 75, pp. 103–112, 2014, doi: 10.1016/j.tws.2013.10.015.

[20] N.D. Duc and P.T. Thang, "Nonlinear buckling of imperfect eccentrically stiffened metal–ceramic–metal S-FGM thin circular cylindrical shells with temperature-dependent properties in thermal environments," *Int. J. Mech. Sci.*, vol.81, pp. 17–25, 2014, doi: 10.1016/j.ijmecsci.2014.01.016.

[21] N.D. Duc, N.D. Tuan, T.Q. Quan, N.V. Quyen, and T.V. Anh, "Nonlinear mechanical, thermal and thermo-mechanical post-buckling of imperfect eccentrically stiffened thin FGM cylindrical panels on elastic foundations," *Thin-Walled Struct.*, vol. 96, pp. 155–168, 2015, doi: 10.1016/j.tws.2015.08.005.

[22] D.H. Bich and H. Van Tung, "Non-linear axisymmetric response of functionally graded shallow spherical shells under uniform external pressure including temperature effects," *Int. J. Nonlinear Mech.*, vol. 46, no. 9, pp. 1195–1204, 2011, doi: 10.1016/j.ijnonlinmec.2011.05.015.

[23] A.H. Sofiyev, A.M. Najafov and N. Kuruoğlu, "The effect of non-homogeneity on the non-linear buckling behavior of laminated orthotropic conical shells," *Compos. B. Eng.*, vol. 43, no. 3, pp. 1196–1206, 2012, doi: 10.1016/j.compositesb.2011.10.010.

[24] M. Bohlooly, and K. Malekzadeh Fard, "Buckling and postbuckling of concentrically stiffened piezo-composite plates on elastic foundations," *J. Appl. Comput. Mech.*, vol. 5, no. 1, pp. 128–140, 2019, doi: 10.22055/JACM.2018.25539.1277.

[25] K. Foroutan and L. Dai, "Static and dynamic thermal post-buckling analysis of imperfect sigmoid FG cylindrical shells resting on a non-uniform elastic foundation," *Eur. J. Mech. A Solids*, vol. 97, 104770, 2023, doi: 10.1016/j.euromechsol.2022.104770.

[26] S. Zhu, Z. Tong, J. Sun, Q. Li, Z. Zhou, and X. Xu, "Electro-thermo-mechanical post-buckling of piezoelectric functionally graded cylindrical shells," *Appl. Math. Model.*, vol. 98, pp. 309–322, 2021, doi: 10.1016/j.apm.2021.05.011.

[27] R.M. Jones, *Mechanics of composite materials*. CRC press, 2018.

[28] M. Bohlooly and B. Mirzavand, "Postbuckling and deflection response of imperfect piezo-composite plates resting on elastic foundations under in-plane and lateral compression and electro-thermal loading," *Mech. Adv. Mater. Struct.*, vol. 25, no. 3, pp. 192–201, 2018, doi: 10.1080/15376494.2016.1255818.

[29] M. Bohlooly, B. Mirzavand, and K. Malekzadeh Fard, "An analytical approach for postbuckling of eccentrically or concentrically stiffened composite double curved panel on nonlinear elastic foundation," *Appl. Math. Model.*, vol. 62, pp. 415–435, 2018, doi: 10.1016/j.apm.2018.06.008.

[30] K. Malekzadeh Fard and M. Bohlooly, "Postbuckling of piezo-laminated cylindrical shells with eccentrically/concentrically stiffeners surrounded by nonlinear elastic foundations," *Compos. Struct.*, vol. 171, pp. 360–369, 2017, doi: 10.1016/j.compstruct.2017.03.058.

[31] P.R. Everall and G.W. Hunt, "Arnold tongue predictions of secondary buckling in thin elastic plates," *J. Mech. Phys. Solids*, vol. 47, no. 10, pp. 2187–2206, 1999, doi: 10.1016/S0022-5096(99)00008-3.

[32] M. Bohlooly Fotovat, T. Kubiak, and P. Perlikowski, "Mixed mode nonlinear response of rectangular plates under static and dynamic compression," *Thin-Walled Struct.*, vol. 184, 110542, 2023, doi: 10.1016/j.tws.2023.110542.

[33] M. Urbaniak, J. Świniarski, P. Czapski, and T. Kubiak, "Experimental investigations of thin-walled GFRP beams subjected to pure bending," *Thin-Walled Struct.*, vol. 107, pp. 397–404, 2016, doi: 10.1016/j.tws.2016.06.022.

[34] P. Czapski, "Influence of laminate code and curing process on the stability of square cross-section, composite columns – Experimental and FEM studies," *Compos. Struct.*, vol. 250, pp. 112564, 2020, doi: 10.1016/j.compstruct.2020.112564.